Magneto-mechanically induced antimicrobial properties of cone-like shaped surfaces

Jorge Marqués-Marchán [a,*], Margarida M. Fernandes [b,c], Senentxu Lanceros-Méndez [c,d,e], Agustina Asenjo [a,*]

[a] *Instituto de Ciencia de Materiales de Madrid, CSIC, Madrid 28049, Spain*
[b] *Centre of Biological Engineering, University of Minho, Campus de Gualtar, Braga 4710-057, Portugal*
[c] *Physics Centre of Minho and Porto Universities (CF-UM-UP) and Laboratory of Physics for Materials and Emergent Technologies (LapMET), University of Minho, Braga 4710-057, Portugal*
[d] *BCMaterials, Basque Center for Materials, Applications and Nanostructures, UPV/EHU Science Park, Leioa 48940, Spain*
[e] *Ikerbasque, Basque Foundation for Science, Bilbao 48009, Spain*

A B S T R A C T

Hygienic surfaces that prevent the proliferation of harmful microorganisms are required in a large variety of environments, including medical areas. Novel strategies are being developed to impede microorganisms colonization of surfaces. In this work, Terfenol-D cone-like shaped nanopatterned surfaces are fabricated by sputtering. The bactericidal effect of such surfaces owed to their morphology is increased in combination with an alternating magnetic field, which boosts the mechanical injury caused to the planktonic cells. Bactericidal assays with Gram-negative *Escherichia coli* are carried out under static (i.e. without any external stimuli) and dynamic (under the application of an alternating magnetic field) conditions for control silicon substrates, Terfenol-D films and nanostructured surfaces. The nanostructured surfaces at the dynamic condition exhibit the larger bactericidal effect. Bacterial adhesion on the materials was analyzed, and results show a reduction of the attachment surface of bacterial cells on Terfenol-D surfaces in comparison with the control silicon that are attributed both to material properties and nanostructuration. Thus, this work exhibits a method to induce and/or improve the mechanical antimicrobial behavior of surfaces via application of a magnetic field, as an alternative or in combination with chemical methods, which are losing effectiveness due to the increase of antibiotic resistance.

1. Introduction

Medical devices, such as implants, laboratory or surgical instruments usually present large metallic or non-metallic surfaces exposed to potentially contaminated environments. A common problem that may arise from the use of these tools is the proliferation of pathogenic microorganisms and biofilm formation on their surface, which can lead to healthcare-associated infections (HAIs) [1]. Nosocomial infections cause difficulties in patients that can vary from minor symptoms to sepsis and even death [2]. Since few microbes are enough to colonize the surface, contamination can occur quickly after their disinfection or even remain after cleaning [3,4]. Hence, novel strategies to prevent the adhesion of bacteria and thus the biofilm formation are needed. Combined physical approaches such as antimicrobial nanocoatings and nanostructuration have been growingly addressed as an alternative to chemical approaches

(bactericidal agents, antimicrobials, antibiotics) in order to prevent the alarming increase in antimicrobial resistance.

For example, electroactive materials have been proven to possess antibacterial properties through the development of electric microenvironments at their surface [5]. Due to the negatively charged nature of bacteria, positively charged nanostructures can disrupt bacterial membranes and hinder their proliferation by contact killing [6–8]. In particular, ceramics materials with electrically charged interfaces and surface microroughness have been demonstrated to achieve a high antibacterial efficacy [9].

Nanostructured surfaces are proposed for killing bacteria mechanically by penetrating and destroying their membranes or by hindering their adhesion [10,11]. Some of these surfaces can be found in nature on some plants and insects, as cicada wings, which exhibit nanoneedles or nanopillars arrays with heights of 200 nm, diameters of 60 nm at the top

---

and 100 nm at the bottom of the nanopillars, and interspacing of 170 nm [12]. Bacteria can colonize microstructured surfaces if their morphological features are similar or larger than bacteria sizes, while in nanostructured surfaces the contact area of bacteria with the substrate is reduced due to the decreased number of attachment points [10,13,14]. In addition to the antifouling properties, these nanostructured surfaces (whose elements desirably have a high aspect-ratio) present a mechano-bactericidal behavior by stretching bacterial cell membranes over their elastic limit, inducing their lysis. Theoretical elastic models have been developed to describe the underlying mechanisms [15–17]. A simple model considers a rigid nanopatterned substrate and takes into account the bacteria elastic modulus and four geometrical factors of the nanostructured surface: nanopillar diameter, base diameter, height and distance between elements [10].

Thus, nanostructured surfaces with different mechanical characteristics have been evaluated with respect to their bactericidal activity. Ordered silicon nanopillar arrays with different heights exhibited the highest bactericidal activity for an intermediate pillar height of around 360 nm as nanopillar elasticity contributes to decrease bacterial adhesion. Notice that the contact area increases both for lower heights (220 nm), and thus more rigid nanopillars, and for longer nanopillars (420 nm) since they adhered, forming clusters [18]. Similarly, gold nanofeatures with different shapes (pillars, rings and nuggets) and same sizes grown on a metallic layer show similar bactericidal response with Gram-positive *Staphylococcus aureus* [19]. Aluminum alloy 6063 surfaces with randomly oriented nanofeatures also demonstrated antibacterial and antiviral properties apart from being durable under mechanical loads [20]. As a way to improve the antimicrobial activity, these surfaces can additionally be functionalized. For instance, nanocolumnar titanium coatings have shown a better performance after the combination with tellurium nanorods [21], and nanostructured surfaces with salt-responsive bacterial releasing behavior are able to remove bacteria debris, maintaining the mechanobactericidal activity [22].

In a more recent approach, dynamic strategies have been used. The application of an external mechanical vibration to piezoelectric polymer surfaces, either positively or negatively charged, promotes the antifouling and antiadhesive characteristics [5]. In a similar approach, magnetoelectric nanocomposites have also shown antimicrobial properties under an external magnetic stimulus [23]. Magnetostrictive microactuators have been proposed to act remotely by external magnetic fields for cell studies and intracellular applications [24]. Magneto-mechanically actuated microstructures have also shown to inhibit bacterial biofilm formation [25].

In this work, we propose to combine the antibacterial properties of the nanostructured surfaces and the magneto-mechanically active nanostructures. In particular, the antimicrobial activity of magnetostrictive ordered conical nanopillars arrays is examined under the application of an external alternating magnetic field. Ordered nanostructured surfaces have shown better anti-biofouling effects than randomly oriented nanosized surfaces [26,27]. The geometry of the nanostructures has been selected in order to optimize the bactericidal effect [28]. Instead of a standard metal, Terfenol-D is used for the fabrication of the nanostructures due to its biocompatibility and giant magnetostriction coefficients, which range in the order of 10^{-3} for single and polycrystalline structures and of 10^{-4} for amorphous structures [29–33]. Due to the magnetostriction behavior, the nanopillars size is modified accordingly to the magnetic field changes and magnetically induced mechano-bactericidal activity is therefore enhanced. Another great advantage of this procedure is the possibility to boost this antimicrobial activity remotely by a magnetic field, what could be employed in medical devices when needed, even in an inserted implant.

2. Experimental section

Materials: Terfenol-D ($Tb_{0.3}Dy_{0.7}Fe_{1.9}$) sputtering target was purchased from Testbourne Ltd. Silicon (Si) wafers were supplied by MicroChemicals. Porous masks with pore diameter of 450 nm and interpore distance of 950 nm, with hydrophobic coating, were acquired from Aquamarijn Micro Filtration BV. Gram-negative *Escherichia coli* (*E. coli*) K-12 were obtained from American Type Culture Collection (LGC Standards S.L.U) and were used in all antimicrobial assays.

Samples Preparation: Terfenol-D samples were grown using DC magnetron sputtering in high vacuum conditions with an argon pressure of 4.6×10^{-3} mbar. The deposition rate was of approximately 1 Å/s, and around 700 nm of Terfenol-D were deposited onto silicon substrates. During the deposition, an in-plane magnetic field of 190 mT is applied continuously by a set of magnets. Before the Terfenol-D deposition, a thin film of titanium of 2 nm was sputtered on silicon in order to improve the adhesion of the material. Two types of Terfenol-D samples were grown under these same conditions: thin films and nanostructured surfaces. For the latest, porous masks were adhered on the Si substrates with Kapton tape and removed after the deposition. A schematic representation of the fabrication process and conditions is shown in Fig. 1. Detailed information about the general dimensions of the samples is presented in Supporting Information Section 1.

Samples Characterization: Magnetic hysteresis loops of Terfenol-D thin films were measured by magneto-optic Kerr effect (MOKE, Nano-MOKE®2 Kerr effect magnetometer) and a superconducting quantum interference device (SQUID, Quantum Design MPMS-5S), and hysteresis loops of the nanostructured surfaces were obtained by vibrating sample magnetometry (VSM, ADE system EV7 KLA-Tencor). Surface morphology of the patterned samples were characterized by scanning electron microscopy (SEM, FEI VERIOS 460), and the roughness of Terfenol-D thin films was evaluated by atomic force microscopy (AFM) with a Nanotec Scanning Probe Microscopy system controlled by the WSxM software [34], using a Nanosensors PPP-FMR probe.

Magnetostriction simulations: The magnetostriction behavior of the Terfenol-D pillars and films was evaluated performing COMSOL [35] simulations. The modeling details and the results obtained are included in Supporting Information Section 2.

Antimicrobial assays: For evaluating the antimicrobial activity, apart from the Terfenol-D thin films and nanopatterned surface samples, Si substrates were used as control material. Materials were sterilized with UV light for 15 min on each side. The *E. coli* bacteria pre-inoculum was achieved by placing a single colony from the culture stock in nutrient broth and incubated overnight at 37 °C and 110 rpm. Afterwards, the pre-inoculum was centrifuged at 5000 rpm for 5 min, to obtain a pellet with bacteria which was further resuspended with NaCl (0.9%) twice. The optical density of the NaCl bacterial suspension was measured at 600 nm (OD_{600}) and then adjusted to 0.36 ± 0.01, which corresponds to approximately 1×10^6 colony-forming units per milliliter ($CFU \cdot mL^{-1}$). A drop of 20 µL of bacterial suspension was placed in contact with the material, previously adhered at the bottom of a 24-well plate (non-treated tissue polystyrene plates (VWR)) with carbon tape. Bacteria were left to grow for 1 hour at 37 °C for static and dynamic conditions. In the dynamic conditions, a variable magnetic field was applied to the materials with a lab-made magnetic bioreactor system [23,36]. In this bioreactor, the magnets below the plate move horizontally with a frequency of 1 Hz and a displacement of 12 mm, allowing a change in the magnetic field from 0 to 23 mT within the culture wells. In the static condition, bacteria were not exposed to any external factors.

Bactericidal activity: The viability of bacterial cells in the drop over the materials following the experiments under static and dynamic conditions was assessed using a colony-forming units (CFUs) assay. The drop was carefully removed from each well with ten-fold serial dilutions in phosphate buffer solution (PBS). For each dilution, a volume of 100 µL was dropped on a NB (Nutrient Broth) plate agar and next incubated at 37 °C for 24 h. Following, the number of viable bacteria was determined, allowing a quantitative analysis of the average $CFU \cdot mL^{-1}$. The bactericidal activity was evaluated with three independent assays as $\log_{10}$ reduction for each condition and compared with that of cells incubated without any material, only with NB.
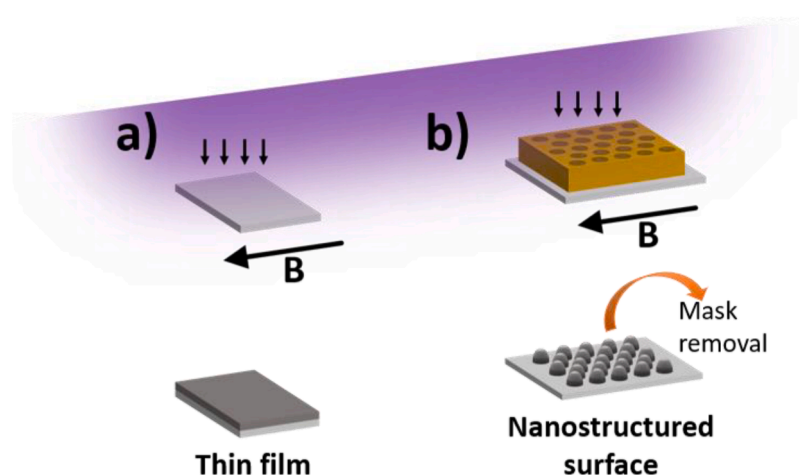
Fig. 1. Scheme of the sample growth procedure. Terfenol-D is sputtered over Si substrates while a magnetic field (B) is applied parallel to their surface, obtaining: (a) thin films, and (b) nanostructured surfaces (using a mask). The arrows above B indicate the in-plane direction of the magnetic field, and the sputtering plasma is depicted as a purple gradient.

Bacterial $\log_{10}$ reduction was calculated as the difference between the number of surviving bacteria over the material (B) and the control (A), which is the bacteria freely growing on the well from the 24 well plate, according to Eq. (1):

$$\text{Bacterial } \log_{10} \text{ reduction} = \log_{10}\left(CFUs\ (A)\right) - \log_{10}\left(CFUs\ (B)\right) \quad (1)$$

Bacterial adhesion: SEM visualization: After removing the drop from the samples, the material was analyzed by microscopy (SEM). In order to allow SEM imaging of the bacteria adhered to the samples surface after bacteria growth, they were washed with PBS solution followed by a fixation step with 3% (v/v) glutaraldehyde for 30 min, and washed again with PBS. Bacteria were further dehydrated with ethanol with increasing concentrations [30, 50, 80, 90 and 100% (v/v)]. Finally, they were coated with 10 nm of gold with a sputter coater Quorum Q130R S and their surface was visualized with a SEM FEI VERIOS 460.

Data Analysis: The results are exhibited as averages with the respective standard deviations. Results were analyzed by GraphPad Prism version X for Windows (GraphPad Software, San Diego, CA, U.S.A.). To determine the statistical significances, one-way analysis of variance, followed by the Dunnett post-hoc test or by the unpaired two-tailed Student's *t*-test method were used.
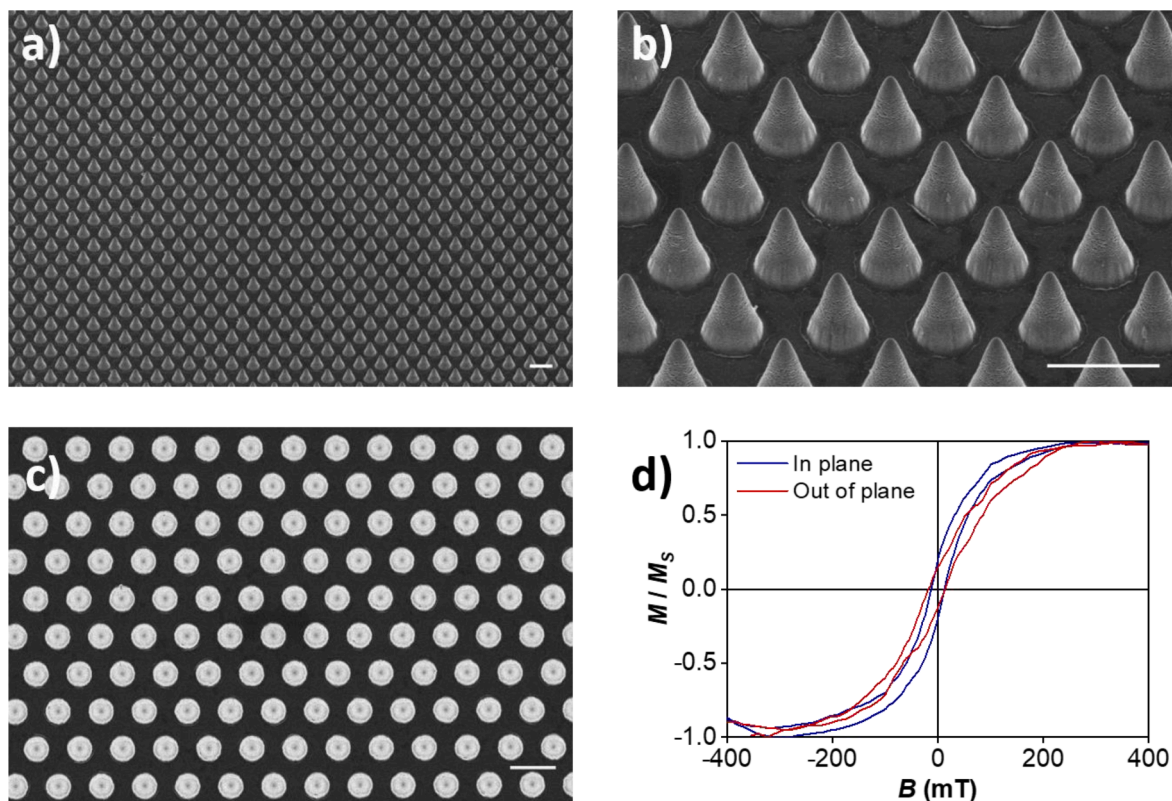

Fig. 2. Characterization of Terfenol-D samples: SEM images of nanostructured surfaces (a), (b) with a tilted angle of 45° from the surface normal and (c) top view; (d) hysteresis loops of nanopatterned surfaces measured along the in-plane direction (parallel to the magnetic field applied during the sputtering) and the out-of-plane direction. Scale bar in all images is of 1 μm.

3. Results and discussion

3.1. Terfenol-D thin films and nanostructured surfaces fabrication and characterization

During sputtering growth, an in-plane magnetic field was applied in order to induce the easy axis of magnetization in that direction [37–39] and thus enhance the magnetostriction coefficient in the out of plane direction with respect to the substrate surface [40]. As shown in Supporting Information Section 3, the in-plane remanence magnetization of the thin film increases from 0.5 to 0.9 M_S (saturation magnetostriction) when the magnetic field is applied during the deposition. Similarly, the remanence magnetization of the nanopatterned surfaces increases from 0.1 to 0.2 M_S due to the enhancement of the in-plane magnetic anisotropy.

Due to the balance between shape and induced anisotropy, both in-plane and out-of-plane hysteresis loops of the Terfenol-D nanopatterned surfaces grown under in-plane magnetic field (Fig. 2d) present similar behavior, with a coercivity of 14 mT.

Terfenol-D thin films were characterized by atomic force microscopy (AFM), presenting a flat surface with an RMS roughness value of 0.2 nm (Supporting Information Section 4). The surface morphology of the nanopillars is displayed by the SEM images in Fig. 2a-c. Each element of the surface has a cone-like pillar shape with approximately basis of 550 nm in diameter, 700 nm in height, and tip diameter of 90 nm. The nanopillars are arranged in a hexagonal array with a distance of 950 nm between centers. These dimensions match with the sizes reported in literature to possess bactericidal properties, with nanopatterns where the elements have a high aspect ratio [28].

Due to the magnetostriction properties of the Terfenol-D, the estimated elongation along the out of plane direction within the bactericidal assays conditions (around 23 mT applied perpendicularly to the substrates) is around 0.03 nm for the thin films and of 0.2 nm for the pillars (Supporting Information Section 2). This difference of one order of magnitude is attributed to the geometry of the samples. The conical shape of the pillars, which get thinner along their height, facilitates to achieve a higher elongation at their apices. Additional effects due to the magnetic field gradients are negligible in comparison with the magnetostriction effect as shown in Supporting Information S2.

3.2. Antimicrobial properties

The bactericidal activity of the materials was assessed towards the clinically relevant Gram-negative bacterium *E. coli*. According to the latest data published in The Lancet, this bacterium is one of the six leading pathogens for deaths associated with antimicrobial resistance [41]. The assays were performed under static (without any external excitation) and dynamic (under an alternating magnetic field) conditions. The employed bioreactor for the dynamic condition ensures the control of the alternating magnetic field by the movement of permanent magnets [36], as an alternative to the control through electromagnetic coils [42]. The magnetic field values used in this work (ranging from 0 to 23 mT) are acceptable for being applied to biological systems and are affordable for the application at large scale to general systems, for both in vitro and in vivo assays.

E. coli adhesion response for the cone-shaped Terfenol-D surfaces and their combination with the application of a magnetic field was then studied for 1 h after dropping a saline solution containing bacteria onto the nanopatterned surface. Silicone biomaterials are commonly used in current medical devices and therefore were selected as a control material. By comparing the different studied structures, it can be observed that both Terfenol-D films and cone-shaped pillars induce an important bacterial cell reduction in solution when compared with the control material silicon and the control (bacterial solution without any material). In fact, the solution in the presence of control silicon presents approximately the same number of bacteria when compared to the

bacterial control solution (Fig. 3). At static conditions, i.e. without the application of magnetic field, the Terfenol-D films and cone-shaped pillars induce a reduction of approximately 2 $\log_{10}$ CFUs/mL, statistically different when compared with the control silicon (*$P < 0.05$). Upon application of the magnetic stimuli, the reduction is more expressive in the pillars inducing nearly 3 $\log_{10}$ CFUs/mL, while in the case of the films the reduction is around 1.5 $\log_{10}$ CFUs/mL (Fig. 3). The difference on the bacterial reduction on the pillars between static and dynamic conditions is found to be statistically significant (**$P < 0.01$), highlighting the improved bactericidal effect upon application of the stimuli.

SEM images in Fig. 4 are displayed to visualize the substrate adhesion and morphology of the bacteria at the studied conditions. It is observed that over silicon control (Figs. 4c and 4f), the integrity of bacteria is maintained although over Terfenol-D films and pillars, the bacteria seem highly compromised (Figures 4, S5.1 and S5.2). At static conditions over the Terfenol-D films (Fig. 4b and Figure S5.2), *E. coli* cell membranes look disrupted as they present holes in their morphology and, more remarkably, the bacteria do not recline on these surfaces, reducing the contact area. In the nanostructured surfaces, at static conditions, the contact area of the bacteria on the substrate is as well reduced, as they only lay over the tip of the pillars (Fig. 4a). Thus, Terfenol-D films and patterned geometry exhibit antifouling properties. These results are in good agreement with the bactericidal activity assays (Fig. 3), where it is observed a reduction of 2 $\log_{10}$ CFUs/mL for both cases. Thus, in the case of Terfenol-D, the chemical characteristic of the material imposes to morphology features in its antifouling behavior (see Fig. 5). In contrary, as seen in Figure S5.2, the bacteria membranes lay over the silicon for both static and dynamic conditions.

Upon application of the magnetic field, the bacterial adhesion appears to be promoted at the surface of the Terfenol-D film, since a biofilm is observed in the SEM images (Fig. 4e). Further, cell viability is around 1 $\log_{10}$ CFUs/mL higher compared to the same surface under static conditions (Fig. 3). The magnetostriction of Terfenol-D seems to tailor the adhesion of bacteria upon magnetic field application, similarly to what occurs upon mechanoelectric stimulation reported by Carvalho et al. [5]. In this case, we have a magnetomechanical stimulus in which the Terfenol-D substrate oscillates with an amplitude of the order of 0.03 nm (Supporting Information Section 2). Sub-micro and nano
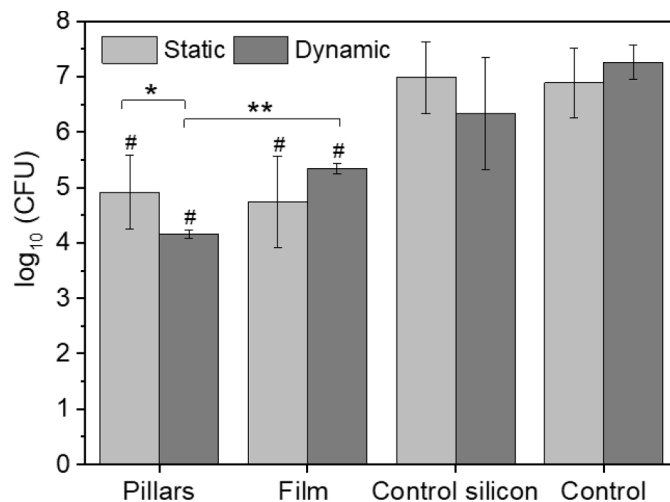

Fig. 3. Planktonic cell viability of the bacterial cells after the assays for different conditions (static and dynamic) and samples: Terfenol-D nanostructured pillars surface, Terfenol-D thin film, control silicon and control (bacterial solution without any material). The symbols (asterisks and cardinals) represent the statistical differences between the different groups of samples: #$P < 0.05$ when compared with each control; *$P < 0.05$ between static and dynamic condition in pillars material; **$P < 0.01$ between the pillars and films at dynamic conditions.
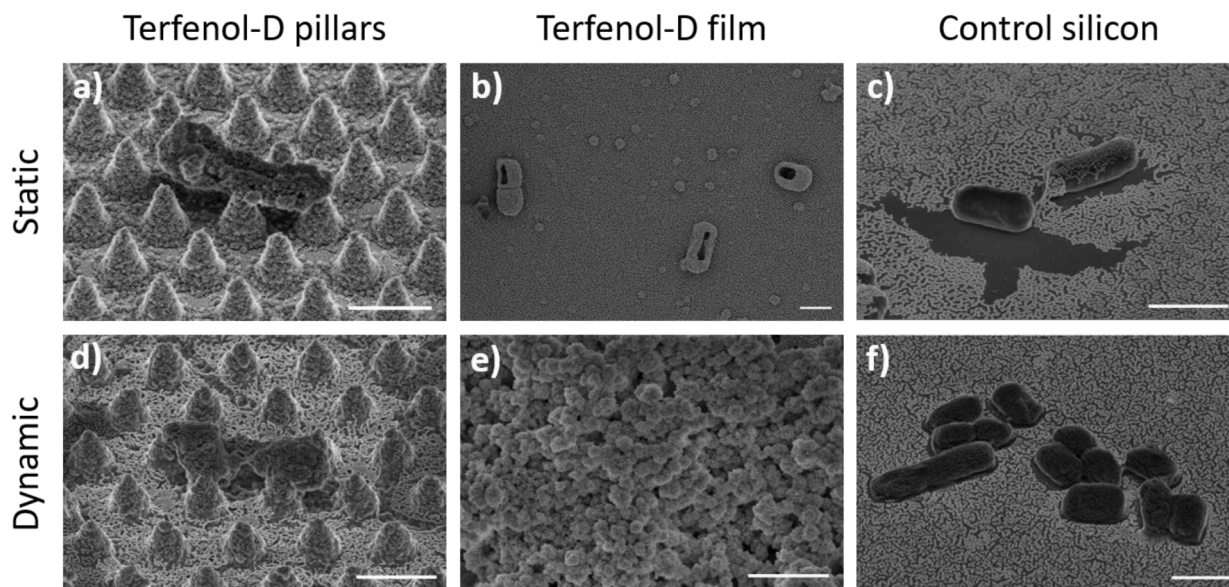
Fig. 4. SEM images of bacteria on the materials after the assays. Each image corresponds to a different condition (first row: static, second row: dynamic) and material (Terfenol-D pillars, film and silicon) as indicated. Scale bar in all images is of 1 μm.
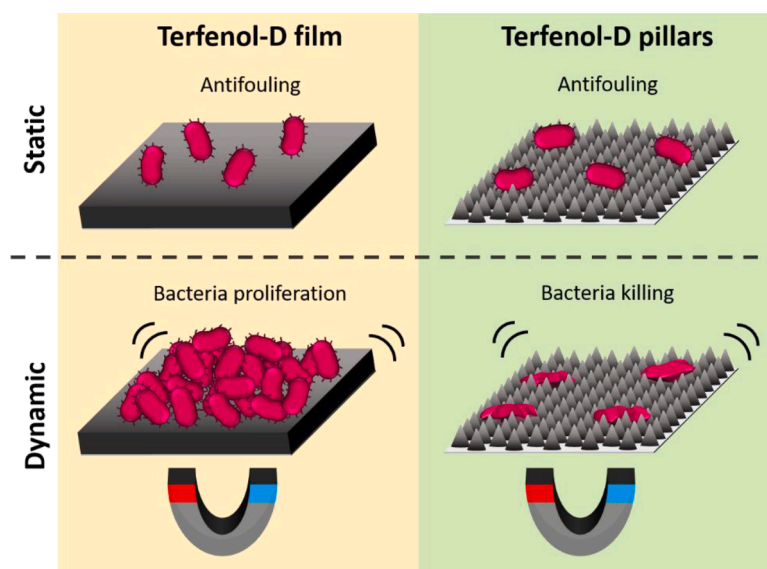

Fig. 5. Schematic representation of the bacteria response for the different Terfenol-D surfaces (flat films and pillar-shaped nanopatterned) under static (without any stimuli) and dynamic (with an alternating magnetic field leading to magneto-mechanical action) conditions.

mechanical vibrations have demonstrated to be capable of tailoring bacteria proliferation on different materials [43,44]. Kazan et al. and Kopel et al. assessed the bactericidal action of low-energy acoustic waves (amplitudes between 0.2 and 2 nm) for different kind of bacteria, such as *E. coli* and *Pseudomonas aeruginosa* [45,46]. In a different work, Wang et al. reported that ultrasonic vibrations with amplitudes from 0.05 nm exhibit an antimicrobial behavior [47]. In this work, Terfenol-D films oscillation at 1 Hz stimulates bacteria growth (Fig. 5). The application of such frequencies may trigger the proliferation of bacteria attached to these surfaces, due to the already reported effect of depolarization of the bacterial membrane of *E. coli* [48]. This phenomenon is governed by a mechanotransduction mechanism that allows increased influx of calcium ions, thus resulting in improved proliferation [5]. Nevertheless, the proliferation seems to occur only in the surface of the material, due to the proximity of the applied stimuli, since in Fig. 3 it has been observed a slight reduction on the viability of bacteria that grow in

suspension over the material, most probably due to the resulting nutrient-poor environment in solution. This effect has also been observed previously by Carvalho et al. [5] in *E. coli* upon mechanical stimulation of piezoelectric polyvinylidene fluorides films.

At dynamic conditions, the pillars kill bacteria by poking and destroying their membranes. In these patterned surfaces, the mechanical elongation of the pillars together with the application of the magnetic field induce a complete lysis of the cells, presenting a completely "melted" structure over the pillars, also being visualized debris of the cells all over the surface (Figs. 4d and 5). Pillars magnetostriction origins a vertical oscillation of the order of 0.2 nm, which aids the penetration of their tips into bacteria membranes. Hence, the magnetostrictive action increases the geometrical bactericidal properties, which kill bacteria by themselves in a mechanism of action already proven for different nanostructures [10,49]. Further images reinforcing these results are provided in Supporting Information Section 5.

4. Conclusion

Magnetostrictive Terfenol-D films and ordered nanopatterned surfaces were fabricated by sputtering. Terfenol-D films show a bactericide behavior attributed to the chemical material properties. In the absence of any external stimulus, nanopatterned surfaces present the same bactericide behavior as the films. In these structured surfaces, with a conical shape, the number of attachment points of *E. coli* bacteria on the substrate are decreased due to morphological features. Upon the application of an alternating magnetic field, bacteria proliferate on the films, indicating that their bactericide activity could be tailored. In the case of the nanopatterned surfaces, the combination of the structural configuration with the application of an external alternating magnetic field increases this bactericide effect as the structures jab into bacteria membranes. Under this condition, the magnetostrictive cone-shaped pillars movement boosts the poking effect, achieving the complete lysis of the planktonic cell membranes.

Therefore, from one side, this work demonstrates that the magneto-mechanical antimicrobial activity of flat surfaces can tailor the proliferation of bacteria. From other side, mechanical bactericide action of nanofeatured surfaces can be enhanced by additional stimuli. The employment of a magnetic field allows to provide this stimulus from the distance. Hence, here we present a novel physical method to inhibit microorganisms colonization of surfaces, as an alternative to chemical techniques, which are losing efficacy because of the increasing bacteria resistance to antibiotics. The biocompatibility of the material allows its application in medical devices, such as implants, and the magnetic field would also enable to boost the antimicrobial activity once they are inserted in the patient's body.

Data availability

Data will be made available on request.

Declaration of Competing Interest

The authors declare that they have no known competing financial interests or personal relationships that could have appeared to influence the work reported in this paper.

Data availability

Data will be made available on request.

Acknowledgments

Supplementary materials

Supplementary material associated with this article can be found, in the online version, at doi:10.1016/j.apmt.2023.101900.

References

[1] J.P. Boutrand, Biocompatibility and Performance of Medical Devices, Woodhead Pub, 2012.

[2] C. Boev, E. Kiss, Hospital-Acquired Infections: Current Trends and Prevention, Crit. Care Nurs. Clin. North Am. 29 (2017) 51–65, https://doi.org/10.1016/j.cnc.2016.09.012.

[3] M.P. Muller, C. MacDougall, M. Lim, I. Armstrong, A. Bialachowski, S. Callery, W. Ciccotelli, M. Cividino, J. Dennis, S. Hota, G. Garber, J. Johnstone, K. Katz, A. McGeer, V. Nankoosingh, C. Richard, M. Vearncombe, Antimicrobial surfaces to prevent healthcare-associated infections: A systematic review, J. Hosp. Infect. 92 (2016) 7–13, https://doi.org/10.1016/j.jhin.2015.09.008.

[4] J.A. Otter, M. Cummins, F. Ahmad, C. van Tonder, Y.J. Drabu, Assessing the biological efficacy and rate of recontamination following hydrogen peroxide vapour decontamination, J. Hosp. Infect. 67 (2007) 182–188, https://doi.org/10.1016/j.jhin.2007.07.019.

[5] E.O. Carvalho, M.M. Fernandes, J. Padrao, A. Nicolau, J. Marqués-Marchán, A. Asenjo, F.M. Gama, C. Ribeiro, S. Lanceros-Mendez, Tailoring Bacteria Response by Piezoelectric Stimulation, ACS Appl. Mater. Interf. (2019) 11, https://doi.org/10.1021/acsami.9b05013.

[6] A. Francesko, M.M. Fernandes, K. Ivanova, S. Amorim, R.L. Reis, I. Pashkuleva, E. Mendoza, A. Pfeifer, T. Heinze, T. Tzanov, Bacteria-responsive multilayer coatings comprising polycationic nanospheres for bacteria biofilm prevention on urinary catheters, Acta Biomater. 33 (2016) 203–212, https://doi.org/10.1016/j.actbio.2016.01.020.

[7] M.M. Fernandes, A. Francesko, J. Torrent-Burgués, F.J. Carrión-Fité, T. Heinze, T. Tzanov, Sonochemically processed cationic nanocapsules: Efficient antimicrobials with membrane disturbing capacity, Biomacromolecules 15 (2014) 1365–1374, https://doi.org/10.1021/bm4018947.

[8] M. Arakha, M. Saleem, B.C. Mallick, S. Jha, The effects of interfacial potential on antimicrobial propensity of ZnO nanoparticle, Sci. Rep. 5 (2015), https://doi.org/10.1038/srep09578.

[9] J.J. Reinosa, M.M. Rojo, A. del Campo, M. Martín-González, J.F. Fernández, Highly Efficient Antimicrobial Ceramics Based on Electrically Charged Interfaces, ACS Appl. Mater. Interf. 11 (2019) 39254–39262, https://doi.org/10.1021/acsami.9b10690.

[10] D.P. Linklater, V.A. Baulin, S. Juodkazis, R.J. Crawford, P. Stoodley, E.P. Ivanova, Mechano-bactericidal actions of nanostructured surfaces, Nat. Rev. Microbiol. 19 (2021) 8–22, https://doi.org/10.1038/s41579-020-0414-z.

[11] M. Michalska, F. Gambacorta, R. Divan, I.S. Aranson, A. Sokolov, P. Noirot, P. D. Laible, Tuning antimicrobial properties of biomimetic nanopatterned surfaces, Nanoscale 10 (2018), https://doi.org/10.1039/c8nr00439k.

[12] A. Tripathy, P. Sen, B. Su, W.H. Briscoe, Natural and bioinspired nanostructured bactericidal surfaces, Adv. Colloid Interface Sci. 248 (2017) 85–104, https://doi.org/10.1016/j.cis.2017.07.030.

[13] A. Francone, S. Merino, A. Retolaza, J. Ramiro, S.A. Alves, J.V. de Castro, N. M. Neves, A. Arana, J.M. Marimon, C.M.S. Torres, N. Kehagias, Impact of surface topography on the bacterial attachment to micro- and nano-patterned polymer films, Surfaces and Interfaces 27 (2021), https://doi.org/10.1016/j.surfin.2021.101494.

[14] A. Peter, A.H.A. Lutey, S. Faas, L. Romoli, V. Onuseit, T. Graf, Direct laser interference patterning of stainless steel by ultrashort pulses for antibacterial surfaces, Opt. Laser Technol. 123 (2020), 105954, https://doi.org/10.1016/J.OPTLASTEC.2019.105954.

[15] F. Xue, J. Liu, L. Guo, L. Zhang, Q. Li, Theoretical study on the bactericidal nature of nanopatterned surfaces, J. Theor. Biol. 385 (2015) 1–7, https://doi.org/10.1016/j.jtbi.2015.08.011.

[16] X. Li, Bactericidal mechanism of nanopatterned surfaces, Phys. Chem. Chem. Phys. 18 (2015) 1311–1316, https://doi.org/10.1039/c5cp05646b.

[17] S. Pogodin, J. Hasan, V.A. Baulin, H.K. Webb, V.K. Truong, T.H. Phong Nguyen, V. Boshkovikj, C.J. Fluke, G.S. Watson, J.A. Watson, R.J. Crawford, E.P. Ivanova, Biophysical model of bacterial cell interactions with nanopatterned cicada wing surfaces, Biophys. J. 104 (2013) 835–840, https://doi.org/10.1016/j.bpj.2012.12.046.

[18] E.P. Ivanova, D.P. Linklater, M. Werner, V.A. Baulin, X. Xu, N. Vrancken, S. Rubanov, E. Hanssen, J. Wandiyanto, V.K. Truong, A. Elbourne, S. Maclaughlin, S. Juodkazis, R.J. Crawford, The multi-faceted mechano-bactericidal mechanism of nanostructured surfaces contributed to elastic modeling analysis, Proc. Natl. Acad. Sci. (2020) 117, https://doi.org/10.1073/pnas.1916680117.

[19] S. Wu, F. Zuber, J. Brugger, K. Maniura-Weber, Q. Ren, Antibacterial Au nanostructured surfaces, Nanoscale 8 (2016) 2620–2625, https://doi.org/10.1039/c5nr06157a.

[20] J. Hasan, Y. Xu, T. Yarlagadda, M. Schuetz, K. Spann, P.K.D.V. Yarlagadda, Antiviral and Antibacterial Nanostructured Surfaces with Excellent Mechanical Properties for Hospital Applications, ACS Biomater. Sci. Eng. 6 (2020) 3608–3618, https://doi.org/10.1021/acsbiomaterials.0c00348.

[21] D. Medina-Cruz, M.U. González, W. Tien-Street, M. Fernández-Castro, A. Vernet-Crua, I. Fernández-Martínez, L. Martínez, Y. Huttel, T.J. Webster, J.M. García-Martín, Synergic antibacterial coatings combining titanium nanocolumns and tellurium nanorods, Nanomedicine 17 (2019) 36–46, https://doi.org/10.1016/j.nano.2018.12.009.

[22] Z. Liu, Y. Yi, L. Song, Y. Chen, L. Tian, J. Zhao, L. Ren, Biocompatible mechano-bactericidal nanopatterned surfaces with salt-responsive bacterial release, Acta Biomater. 141 (2022) 198–208, https://doi.org/10.1016/J.ACTBIO.2022.01.038.

[23] M.M. Fernandes, P. Martins, D.M. Correia, E.O. Carvalho, F.M. Gama, M. Vazquez, C. Bran, S. Lanceros-Mendez, Magnetoelectric Polymer-Based Nanocomposites

with Magnetically Controlled Antimicrobial Activity, ACS Appl. Bio. Mater. 4 (2021) 559–570, https://doi.org/10.1021/acsabm.0c01125.

[24] C. Vargas-Estevez, A. Blanquer, P. Dulal, R. Pérez del Real, M. Duch, E. Ibáñez, L. Barrios, G. Murillo, N. Torras, C. Nogués, B.J.H. Stadler, J.A. Plaza, J. Esteve, Study of Galfenol direct cytotoxicity and remote microactuation in cells, Biomaterials (2017) 139, https://doi.org/10.1016/j.biomaterials.2017.05.049.

[25] S. Leulmi Pichot, H. Joisten, A.J. Grant, B. Dieny, R.P. Cowburn, Magneto-mechanically actuated microstructures to efficiently prevent bacterial biofilm formation, Sci. Rep. (2020) 10, https://doi.org/10.1038/s41598-020-72406-8.

[26] C. Díaz, P.L. Schilardi, R.C. Salvarezza, M.F.L. de Mele, Nano/microscale order affects the early stages of biofilm formation on metal surfaces, Langmuir (2007) 23, https://doi.org/10.1021/la700650q.

[27] M. Jung, T. Kim, H. Kim, R. Shin, J. Lee, J. Lee, J. Lee, S. Kang, Design and fabrication of a large-area superhydrophobic metal surface with anti-icing properties engineered using a top-down approach, Appl. Surf. Sci. (2015) 351, https://doi.org/10.1016/j.apsusc.2015.06.024.

[28] K. Modaresifar, S. Azizian, M. Ganjian, L.E. Fratila-Apachitei, A.A. Zadpoor, Bactericidal effects of nanopatterns: A systematic review, Acta Biomater. 83 (2019), https://doi.org/10.1016/j.actbio.2018.09.059.

[29] C. Ribeiro, V. Correia, P. Martins, F.M. Gama, S. Lanceros-Mendez, Proving the suitability of magnetoelectric stimuli for tissue engineering applications, Colloids Surf. B Biointerf. 140 (2016) 430–436, https://doi.org/10.1016/j.colsurfb.2015.12.055.

[30] M.J. Dapino, On magnetostrictive materials and their use in adaptive structures, Struct. Eng. Mech. 17 (2004) 303–329, https://doi.org/10.12989/sem.2004.17.3_4.303.

[31] F. Schatz, M. Hirscher, M. Schnell, G. Flik, H. Kronmüller, Magnetic anisotropy and giant magnetostriction of amorphous TbDyFe films, J. Appl. Phys. (1994) 76, https://doi.org/10.1063/1.357192.

[32] E. Quandt, Multitarget sputtering of high magnetostrictive Tb-Dy-Fe films, J. Appl. Phys. (1994) 75, https://doi.org/10.1063/1.355626.

[33] A.E. Clark, Chapter 7 Magnetostrictive rare earth-Fe2 compounds, Handb. Ferromagn. Mater. 1 (1980) 531–589, https://doi.org/10.1016/S1574-9304(05)80122-1.

[34] I. Horcas, R. Fernández, J.M. Gómez-Rodríguez, J. Colchero, J. Gómez-Herrero, A. M. Baro, WSXM: A software for scanning probe microscopy and a tool for nanotechnology, Rev. Sci. Instrum. (2007) 78, https://doi.org/10.1063/1.2432410.

[35] COMSOL Multiphysics® v. 6.0, www.comsol.com, COMSOL AB, Stockholm, Sweden.

[36] N. Castro, Fernandes.M.M. Fernandes, C. Ribeiro, V. Correia, R. Minguez, S. Lanceros-Méndez, Magnetic Bioreactor for Magneto-, Mechano- and Electroactive Tissue Engineering Strategies, Sensors 20 (2020), https://doi.org/10.3390/s20123340.

[37] J. Chen, J. Ma, L. Wu, Y. Shen, C.W. Nan, Magnetic anisotropy of Fe films deposited by dc magnetron sputtering under an external magnetic field, Sci. Bull. 60 (2015) 1214–1217, https://doi.org/10.1007/s11434-015-0830-z.

[38] M. Coïsson, W. Hüttenes, M. Cialone, G. Barrera, F. Celegato, P. Rizzi, Z.H. Barber, P. Tiberto, Measurement of thin film magnetostriction using field-dependent atomic force microscopy, Appl. Surf. Sci. 525 (2020), https://doi.org/10.1016/j.apsusc.2020.146514.

[39] K. Zhao, Y. Zhang, G. Pei, J. Luo, B. Ma, Effects of the Bias Magnetic Field and Annealing on the Magnetization of Terfenol-D Films, in: Proceedings of IEEE Sensors, Institute of Electrical and Electronics Engineers Inc., 2022. https://doi.org/10.1109/SENSORS52175.2022.9967057.

[40] B.D. Cullity, C.D. Graham, Introd. Magn. Mater. (2007).

[41] C.J.L. Murray DPhil, K.S. Ikuta, F. Sharara, L. Swetschinski, G.R. Aguilar, A. Gray, C. Han, C. Bisignano, P. Rao, E. Wool, S.C. Johnson, A.J. Browne, M.G. Chipeta, F. Fell, S. Hackett, G. Haines-Woodhouse, B.H.K. Hamadani, E.A.P. Kumaran, B. McManigal, R. Agarwal, S. Akech, S. Albertson, J. Amuasi, J. Andrews, A. Aravkin, E. Ashley, F. Bailey, S. Baker, B. Basnyat, R. Bender, A. Bethou, J. Bielicki, S. Boonkasidecha, J. Bukosia, C. Carvalheiro, C. Castañeda-Orjuela, V. Chansamouth, S. Chaurasia, S. Chiurchiù, F. Chowdhury, A.J. Cook, B. Cooper, T.R. Cressey, E. Criollo-Mora, M. Cunningham, S. Darboe, N.P.J. Day, M. de Luca, K. Dokova, A. Dramowski, S.J. Dunachie, T. Eckmanns, D. Eibach, A. Emami, N. Feasey, N. Fisher-Pearson, K. Forrest, D. Garrett, P. Gastmeier, A.Z. Giref, R. C. Greer, V. Gupta, S. Haller, A. Haselbeck, S.I. Hay, M. Holm, S. Hopkins, K. C. Iregbu, J. Jacobs, D. Jarovsky, F. Javanmardi, M. Khorana, N. Kissoon, E. Kobeissi, T. Kostyanev, F. Krapp, R. Krumkamp, A. Kumar, H.H. Kyu, C. Lim, D. Limmathurotsakul, M.J. Loftus, M. Lunn, J. Ma, N. Mturi, T. Munera-Huertas, P. Musicha, M.M. Mussi-Pinhata, T. Nakamura, R. Nanavati, S. Nangia, P. Newton, C. Ngoun, A. Novotney, D. Nwakanma, C.W. Obiero, A. Olivas-Martinez, P. Olliaro, E. Ooko, E. Ortiz-Brizuela, A.Y. Peleg, C. Perrone, N. Plakkal, A. Ponce-de-Leon, M. Raad, T. Ramdin, A. Riddell, T. Roberts, J.V. Robotham, A. Roca, K.E. Rudd, N. Russell, J. Schnall, J.A.G. Scott, M. Shivamallappa, J. Sifuentes-Osornio, N. Steenkeste, A.J. Stewardson, T. Stoeva, N. Tasak, A. Thaiprakong, G. Thwaites, C. Turner, P. Turner, H.R. van Doorn, S. Velaphi, A. Vongpradith, H. Vu, T. Walsh, S. Waner, T. Wangrangsimakul, T. Wozniak, P. Zheng, B. Sartorius, A.D. Lopez, A. Stergachis, C. Moore, C. Dolecek, M. Naghavi, Global burden of bacterial antimicrobial resistance in 2019: a systematic analysis, Lancet 399 (2022) 629–655, https://doi.org/10.1016/S0140-6736(21)02724-0.

[42] T. Xu, C. Huang, Z. Lai, X. Wu, Independent Control Strategy of Multiple Magnetic Flexible Millirobots for Position Control and Path Following, IEEE Trans. Robot. 38 (2022), https://doi.org/10.1109/TRO.2022.3157147.

[43] S.N. Robertson, P. Campsie, P.G. Childs, F. Madsen, H. Donnelly, F.L. Henriquez, W.G. Mackay, M. Salmerón-Sánchez, M.P. Tsimbouri, C. Williams, M.J. Dalby, S. Reid, Control of cell behaviour through nanovibrational stimulation: Nanokicking, Philos. Trans. A Math. Phys. Eng. Sci. (2018) 376, https://doi.org/10.1098/rsta.2017.0290.

[44] S.N. Robertson, P.G. Childs, A. Akinbobola, F.L. Henriquez, G. Ramage, S. Reid, W. G. Mackay, C. Williams, Reduction of Pseudomonas aeruginosa biofilm formation through the application of nanoscale vibration, J. Biosci. Bioeng. (2020) 129, https://doi.org/10.1016/j.jbiosc.2019.09.003.

[45] Z. Kazan, J. Zumeris, H. Jacob, H. Raskin, G. Kratysh, M. Vishnia, N. Dror, T. Barliya, M. Mandel, G. Lavie, Effective prevention of microbial biofilm formation on medical devices by low-energy surface acoustic waves, Antimicrob. Agents Chemother. 50 (2006), https://doi.org/10.1128/AAC.00418-06.

[46] M. Kopel, E. Degtyar, E. Banin, Surface acoustic waves increase the susceptibility of Pseudomonas aeruginosa biofilms to antibiotic treatment, Biofouling (2011) 27, https://doi.org/10.1080/08927014.2011.597051.

[47] H. Wang, F. Teng, X. Yang, X. Guo, J. Tu, C. Zhang, D. Zhang, Preventing microbial biofilms on catheter tubes using ultrasonic guided waves, Sci. Rep. 7 (2017), https://doi.org/10.1038/s41598-017-00705-8.

[48] G.N. Bruni, R.A. Weekley, B.J.T. Dodd, J.M. Kralj, Voltage-gated calcium flux mediates Escherichia coli mechanosensation, Proc. Natl. Acad. Sci. U.S.A. (2017) 114, https://doi.org/10.1073/pnas.1703084114.

[49] T. Kim, S. Kwon, J. Lee, J.S. Lee, S. Kang, A metallic anti-biofouling surface with a hierarchical topography containing nanostructures on curved micro-riblets, Microsyst. Nanoeng. 8 (2022), https://doi.org/10.1038/s41378-021-00341-3.